DYNAMIC MODELLING, ESTIMATION, AND CONTROL FOR PRECISION POINTING OF AN ATMOSPHERIC BALLOON PLATFORM

David Evan Zlotnik[1], James Richard Forbes[2]
[1]*Research Assistant, Department of Mechanical Engineering, McGill University, Montreal, QC, Canada*
[2]*Assistant Professor, Department of Mechanical Engineering, McGill University, Montreal, QC, Canada*
Email: david.zlotnik@mail.mcgill.ca; james.richard.forbes@mcgill.ca

ABSTRACT

In this paper we consider the dynamic modelling, estimation and control of an atmospheric balloon platform. The platform is modelled as a rigid body constrained to move with a three dimensional pendulum. We investigate the dynamics of the system and derive the equations of motion from first principles. A nonlinear estimator that evolves on the special orthogonal group, denoted $SO(3)$, is implemented and used in conjunction with a proportional derivative (PD) compensator to control the yaw angle of the platform. In addition, a continuous-time Gaussian process disturbance model is used to simulate the effects of disturbances on the platform. A simulation is conducted, and the results demonstrate successful estimation and yaw control.

Keywords: balloon platform modelling, rotation matrix estimation, attitude control.

LA MODÉLISATION DYNAMIQUE, L'ESTIMATION ET LE CONTRÔLE POUR LE GUIDAGE DE PRÉSICION D'UNE PLATEFORME DE BALLON ATMOSPHÉRIQUE

RÉSUMÉ

Dans cet article, on considère la modélisation dynamique, l'estimation et le contrôle d'une plateforme de ballon atmosphérique. La plateforme est modélisée comme un corps rigide contraint de se déplacer avec une pendule à trois dimensions. On examine la dynamique du système et dérive les équations du mouvement à partir des principes fondamentaux. Un estimateur non linéaire qui évolue sur un groupe orthogonal spécial, noté SO(3), est mis en œuvre et utilisé en conjonction avec un compensateur proportionnel dérivé (PD) pour contrôler l'angle de lacet de la plateforme. De plus, on use d'un processus à temps continu Gaussien comme modèle de perturbations pour simuler l'effet du vent sur la plateforme. Une simulation est effectuée et les résultats démontrent la réussite de l'estimation et du contrôle de l'angle de lacet.

Mots-clés : modélisation plateforme de ballon, estimation de la matrice de rotation, contrôle d'attitude.

1. INTRODUCTION

Physicists are concerned with certain properties of the universe, such as the rate at which the universe is expanding. In order to determine the rate at which the universe is expanding, physicists must precisely measure the size of astronomical objects, such as supernova. To do so, ground-based telescopes are used. The accuracy of these telescopes can be greatly improved if properly calibrated using a microwave light source at a known distance and elevation.

The McGill University High Altitude Balloon (McHAB) team has designed, developed and launched a low-cost atmospheric balloon platform that will be used to carry such a microwave light source. However, the balloon platform currently lacks an adequate attitude control system that will enable precision pointing of the microwave light source to be pointed at ground-based telescopes. In this paper the dynamic modelling, estimation and control of such a balloon platform is considered in detail.

Attitude control, that is the control of the orientation and angular velocity of a body, is a nonlinear control problem. The attitude control system must overcome external disturbances, allowing the body to be stabilized and pointed in a desired direction. This requires the use of sensors to estimate the attitude, and actuators to control it [1]. The attitude of a body is completely described by a rotation matrix [2]. However, typically attitude estimation is accomplished by first parameterizing the rotation matrix using a quaternion, and then using an extended Kalman filter to estimate the quaternion [3]. For example, in [4–6] the attitude of a balloon platform is estimated using various sensors and an extended Kalman filter. Despite its popularity, the Kalman filter has been found to perform poorly when adapted to nonlinear systems, especially when coupled with low-cost measurement units [7, 8]. Recently, nonlinear observers that estimate the rotation matrix directly without any sort of quaternion parameterization have been developed [7–10]. The novel contribution of this work is building on [7, 9] by adapting the proposed attitude estimator to the balloon platform being constructed by the McHAB team and observing the performance of the estimator in conjunction with yaw axis feedback control.

The remainder of this paper is as follows. We review notation and give a description of the hardware used on the platform in Sec. 2. In Sec. 3, the kinematics and dynamics of the proposed platform model are considered, and the equations of motion are derived. Sec. 4 is where we review the estimator proposed in [7, 9] and adapt it for use with the balloon platform. We then discuss yaw control and the control algorithm in Sec. 5 and the disturbance model used for the simulation in Sec. 6. We simulate the platform dynamics and present the results in Sec. 7 and close with concluding remarks in Sec. 8.

2. PRELIMINARIES

2.1. Notation

A vector, $\underrightarrow{u}$, can be expressed as

$$\underrightarrow{u} = \underrightarrow{\mathscr{F}}_a^{\mathsf{T}} \mathbf{u}_a,$$

where $\underrightarrow{\mathscr{F}}_a = [\underrightarrow{a}_1 \quad \underrightarrow{a}_2 \quad \underrightarrow{a}_3]^{\mathsf{T}}$ is a reference frame and $\mathbf{u}_a = [u_1 \; u_2 \; u_3]^{\mathsf{T}} \in \mathbb{R}^3$ are the components of $\underrightarrow{u}$ expressed in $\underrightarrow{\mathscr{F}}_a$. The cross product of two vectors can be written as [2]

$$\underrightarrow{u} \times \underrightarrow{v} = \mathbf{u}_a^{\mathsf{T}} \underrightarrow{\mathscr{F}}_a \times \underrightarrow{\mathscr{F}}_a^{\mathsf{T}} \mathbf{v}_a = \underrightarrow{\mathscr{F}}_a^{\mathsf{T}} \mathbf{u}_a^{\times} \mathbf{v}_a$$

where $(\cdot)^{\times} : \mathbb{R}^3 \to \mathfrak{so}(3)$ with [11]

$$\mathfrak{so}(3) = \{\mathbf{S} \in \mathbb{R}^{3\times 3} \mid \mathbf{S}^T = -\mathbf{S}\},$$

such that

$$\mathbf{u}_a^{\times} = \begin{bmatrix} 0 & -u_3 & u_2 \\ u_3 & 0 & -u_1 \\ -u_2 & u_1 & 0 \end{bmatrix}.$$

Given $\underset{\rightarrow}{\mathscr{F}}_b^{\mathsf{T}}\mathbf{v}_b = \underset{\rightarrow}{\mathscr{F}}_i^{\mathsf{T}}\mathbf{v}_i$ the relationship between $\mathbf{v}_b$ and $\mathbf{v}_i$ can be found by taking the dot product with $\underset{\rightarrow}{\mathscr{F}}_b$ to obtain [2],

$$\begin{aligned} \underbrace{\underset{\rightarrow}{\mathscr{F}}_b \cdot \underset{\rightarrow}{\mathscr{F}}_b^{\mathsf{T}}}_{\mathbf{1}}\mathbf{v}_b &= \underset{\rightarrow}{\mathscr{F}}_b \cdot \underset{\rightarrow}{\mathscr{F}}_i^{\mathsf{T}}\mathbf{v}_i \\ \mathbf{v}_b &= \mathbf{C}_{bi}\mathbf{v}_i, \end{aligned}$$

where $\mathbf{C}_{bi} = \underset{\rightarrow}{\mathscr{F}}_b \cdot \underset{\rightarrow}{\mathscr{F}}_i^{\mathsf{T}} \in SO(3)$ is the rotation matrix which transforms the components of a vector from $\underset{\rightarrow}{\mathscr{F}}_i$ to $\underset{\rightarrow}{\mathscr{F}}_b$ and $SO(3)$ denotes the special orthogonal group in $\mathbb{R}^{3\times 3}$ defined as

$$SO(3) = \{\mathbf{C} \in \mathbb{R}^{3\times 3} \mid \mathbf{C}^{\mathsf{T}}\mathbf{C} = \mathbf{1},\ \det(\mathbf{C}) = +1\},$$

where $\mathbf{1}$ is the identity matrix [11].

2.2. McHAB System Overview

The atmospheric ballon system built by the McHAB team is shown in Fig. 1(a). The system consists of a balloon, parachute (to reduce the decent rate), and a platform. The balloon platform is equipped with an inertial measurement unit (IMU) and a Raspberry Pi single-board computer. The IMU is a DIYDrones ArduIMU+ V3, which contains a 3-axis accelerometer, 3-axis gyroscope and a 3-axis magnetometer. Assuming a constant ascent rate, the accelerometer can be used along with the magnetometer and gyroscope for attitude determination. The actuator used for control is a brushless DC motor with a high moment of inertia. This was done to avoid manually machining a flywheel. In this paper, the motor dynamics have been neglected since they operate at a much higher bandwidth. For additional details of the McHAB system see [12].

3. PLATFORM MODEL

Consider the balloon platform model shown in Fig. 1(b). The platform itself is modelled as a rigid body and is denoted $\mathscr{R}$. To model the swinging motion of the platform during flight, we will consider $\mathscr{R}$ to be constrained to move at the end of a pendulum, denoted body $\mathscr{P}$. We model the pendulum as a rigid body. This is reasonable since, in the experience of the McHAB team, the velocity of the balloon will be nonzero during ascent and as such the tether will be in tension. Though $\mathscr{R}$ is constrained to move with the pendulum, it is free to rotate in three dimensions. We attach a reference frame, $\underset{\rightarrow}{\mathscr{F}}_b = [\underset{\rightarrow}{b}_1 \ \ \underset{\rightarrow}{b}_2 \ \ \underset{\rightarrow}{b}_3]^{\mathsf{T}}$, to $\mathscr{R}$ at its centre of mass. Another reference frame, $\underset{\rightarrow}{\mathscr{F}}_p = [\underset{\rightarrow}{p}_1 \ \ \underset{\rightarrow}{p}_2 \ \ \underset{\rightarrow}{p}_3]^{\mathsf{T}}$, is attached to $\mathscr{P}$ with its origin located at the centre of the inertial frame, $\underset{\rightarrow}{\mathscr{F}}_i$. The pendulum $\mathscr{P}$, has one end fixed to the centre of $\underset{\rightarrow}{\mathscr{F}}_i$ and another attached to $\mathscr{R}$ at point o.

3.1. Kinematic Relations and Constraints

In order to describe the motions of the rigid body and pendulum, we require their respective angular velocities. Let $\underset{\rightarrow}{\omega}^{bi} = \underset{\rightarrow}{\mathscr{F}}_b^{\mathsf{T}}\boldsymbol{\omega}_b^{bi}$ and $\underset{\rightarrow}{\omega}^{pi} = \underset{\rightarrow}{\mathscr{F}}_p^{\mathsf{T}}\boldsymbol{\omega}_p^{pi}$ be the angular velocities of $\underset{\rightarrow}{\mathscr{F}}_b$ and $\underset{\rightarrow}{\mathscr{F}}_p$ with respect to $\underset{\rightarrow}{\mathscr{F}}_i$ respectively. The orientation of frames $\underset{\rightarrow}{\mathscr{F}}_b$ and $\underset{\rightarrow}{\mathscr{F}}_p$ with respect to $\underset{\rightarrow}{\mathscr{F}}_i$ can be described by the rotation matrices, $\mathbf{C}_{bi}$ and $\mathbf{C}_{pi}$. These rotation matrices can be defined using any Euler angle sequence, $\boldsymbol{\theta}^{bi} = [\alpha_b \ \ \beta_b \ \ \gamma_b]^{\mathsf{T}}$ or $\boldsymbol{\theta}^{pi} = [\alpha_p \ \ \beta_p \ \ \gamma_p]^{\mathsf{T}}$. We will require the relationship between angular velocity and the

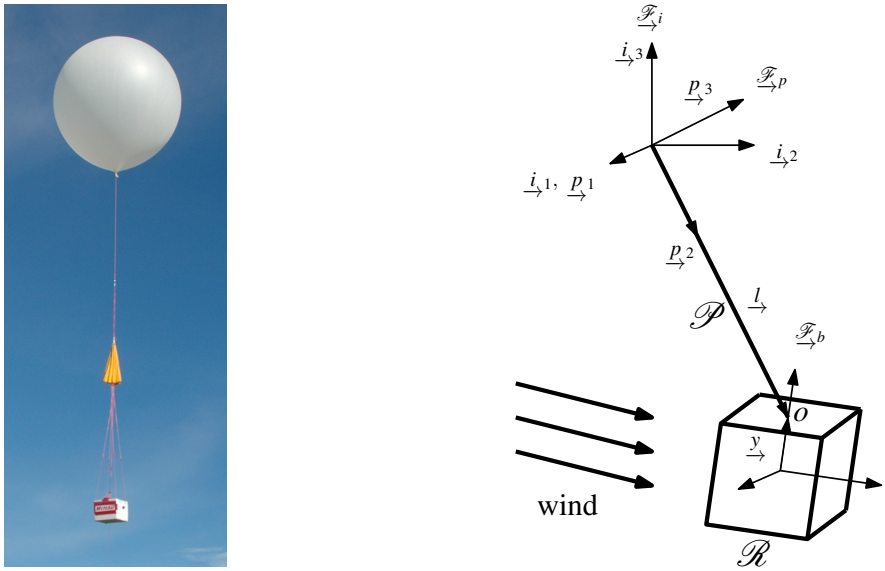

(a) (b)

Fig. 1. (a) Actual balloon platform and (b) platform model

rate of change of the Euler angles [13],

$$\boldsymbol{\omega}_a^{ai} = \mathbf{S}_a^{ai}\dot{\boldsymbol{\theta}}^{ai}, \tag{1}$$

where $\mathbf{S}_a^{ai} = \mathbf{S}_a^{ai}(\alpha_a, \beta_a) \in \mathbb{R}^{3\times 3}$ is the appropriate mapping matrix between the Euler angle rates and the angular velocities, and a replaces b or p. The kinematics of $\mathscr{R}$ and $\mathscr{P}$ are described by [2],

$$\dot{\mathbf{C}}_{bi} + \boldsymbol{\omega}_b^{bi\times}\mathbf{C}_{bi} = \mathbf{0}, \tag{2}$$

and

$$\dot{\mathbf{C}}_{pi} + \boldsymbol{\omega}_p^{pi\times}\mathbf{C}_{pi} = \mathbf{0}$$

respectively.

Constraint Equations

Since we have constrained $\mathscr{R}$ to move with $\mathscr{P}$, the position of $\underrightarrow{\mathscr{F}}_b$ can be described by

$$\underrightarrow{r}^{bi} = \underrightarrow{l} - \underrightarrow{y}$$

where $\underrightarrow{r}^{bi}$ is the position of $\underrightarrow{\mathscr{F}}_b$ with respect to $\underrightarrow{\mathscr{F}}_i$, $\underrightarrow{l}$ is the position of point o with respect to $\underrightarrow{\mathscr{F}}_p$ and $\underrightarrow{y}$ is the position of point o with respect to $\underrightarrow{\mathscr{F}}_b$. Then,

$$\begin{aligned} \underrightarrow{r}^{bi^{\bullet}} &= (\underrightarrow{l}^{\circ} + \underrightarrow{\omega}^{pi} \times \underrightarrow{l}) - (\underrightarrow{y}' + \underrightarrow{\omega}^{bi} \times \underrightarrow{y}) \\ \dot{\mathbf{r}}_i^{bi} &= -\mathbf{C}_{pi}^{\mathsf{T}}\boldsymbol{l}_p^{\times}\boldsymbol{\omega}_p^{pi} + \mathbf{C}_{bi}^{\mathsf{T}}\mathbf{y}_b^{\times}\boldsymbol{\omega}_b^{bi}, \end{aligned} \tag{3}$$

where $(\cdot)^{\bullet}$, $(\cdot)^{\circ}$ and $(\cdot)'$ indicate time derivatives with respect to $\underrightarrow{\mathscr{F}}_i$, $\underrightarrow{\mathscr{F}}_p$ and $\underrightarrow{\mathscr{F}}_b$ respectively. This constraint equation can be written as

$$\underbrace{\begin{bmatrix} \mathbf{1} & -\mathbf{C}_{bi}^{\mathsf{T}}\mathbf{y}_b^{\times}\mathbf{S}_b^{bi} & \mathbf{C}_{pi}^{\mathsf{T}}\boldsymbol{l}_p^{\times}\mathbf{S}_p^{pi} \end{bmatrix}}_{\boldsymbol{\Xi}} \begin{bmatrix} \dot{\mathbf{r}}_b^{bi} \\ \dot{\boldsymbol{\theta}}^{bi} \\ \dot{\boldsymbol{\theta}}^{pi} \end{bmatrix} = \mathbf{0}.$$

Note that in this case $\dot{\mathbf{r}}_b^{bi}$ is dependent on $\dot{\boldsymbol{\theta}}^{bi}$ and $\dot{\boldsymbol{\theta}}^{pi}$. From Eq. (3), we can express $\boldsymbol{\nu} = [\dot{\mathbf{r}}_i^{bi^{\mathsf{T}}} \;\; \boldsymbol{\omega}_b^{bi^{\mathsf{T}}} \;\; \boldsymbol{\omega}_p^{pi^{\mathsf{T}}}]^{\mathsf{T}}$ as

$$\boldsymbol{\nu} = \underbrace{\begin{bmatrix} \mathbf{C}_{bi}^{\mathsf{T}}\mathbf{y}_b^{\times} & -\mathbf{C}_{pi}^{\mathsf{T}}\boldsymbol{l}_p^{\times} \\ \mathbf{1} & \mathbf{0} \\ \mathbf{0} & \mathbf{1} \end{bmatrix}}_{\boldsymbol{\Pi}} \underbrace{\begin{bmatrix} \dot{\boldsymbol{\omega}}_b^{bi} \\ \dot{\boldsymbol{\omega}}_p^{pi} \end{bmatrix}}_{\tilde{\boldsymbol{\nu}}}, \tag{4}$$

and recalling Eq. (1) we can write the above in terms of the Euler angles as

$$\begin{bmatrix} \dot{\mathbf{r}}_i^{bi} \\ \dot{\boldsymbol{\theta}}^{bi} \\ \dot{\boldsymbol{\theta}}^{pi} \end{bmatrix} = \underbrace{\begin{bmatrix} \mathbf{C}_{bi}^{\mathsf{T}}\mathbf{y}_b^{\times}\mathbf{S}_b^{bi} & -\mathbf{C}_{pi}^{\mathsf{T}}\boldsymbol{l}_p^{\times}\mathbf{S}_p^{pi} \\ \mathbf{1} & \mathbf{0} \\ \mathbf{0} & \mathbf{1} \end{bmatrix}}_{\boldsymbol{\Gamma}} \begin{bmatrix} \dot{\boldsymbol{\theta}}^{bi} \\ \dot{\boldsymbol{\theta}}^{pi} \end{bmatrix}.$$

Note that it can be easily verified that,

$$\boldsymbol{\Gamma}^{\mathsf{T}}\boldsymbol{\Xi}^{\mathsf{T}} = \mathbf{0}, \tag{5}$$

a relation that will be of importance later.

3.2. Deriving the Equations of Motion

Both the Lagrangian and the Newton-Euler method can be used to solve for the equations of motion. Here, we will use Lagrange's equation for constrained systems,

$$\frac{d}{dt}\left(\frac{\partial L}{\partial \dot{\mathbf{q}}}\right)^{\mathsf{T}} - \left(\frac{\partial L}{\partial \mathbf{q}}\right)^{\mathsf{T}} = \boldsymbol{\Xi}^{\mathsf{T}}\boldsymbol{\lambda} + \boldsymbol{f}, \tag{6}$$

where $L = T - V$ is the lagrangian, $\mathbf{q}$ are the generalized coordinates, $\boldsymbol{f}$ are the generalized forces, and $\boldsymbol{\lambda}$ are the Lagrange multipliers associated with the constraint equations. In order to formulate the Lagrangian we need to construct the kinetic energy, T, and the potential energy, V, in terms of the generalized coordinates [13],

$$\mathbf{q} = \begin{bmatrix} \mathbf{r}_i^{bi^{\mathsf{T}}} & \boldsymbol{\theta}^{bi^{\mathsf{T}}} & \boldsymbol{\theta}^{pi^{\mathsf{T}}} \end{bmatrix}^{\mathsf{T}}. \tag{7}$$

Kinetic and Potential Energy

The kinetic and potential energy of $\mathscr{R}$ is,

$$T_{\mathscr{R}} = \tfrac{1}{2} m_{\mathscr{R}} \dot{\mathbf{r}}_i^{bi^{\mathsf{T}}} \dot{\mathbf{r}}_i^{bi} + \tfrac{1}{2} \boldsymbol{\omega}_b^{bi^{\mathsf{T}}} \mathbf{I}_{\mathscr{R}} \boldsymbol{\omega}_b^{bi}, \tag{8}$$

and

$$V_{\mathscr{R}} = -m_{\mathscr{R}} g \mathbf{r}_i^{bi^{\mathsf{T}}} \mathbf{1}_3, \tag{9}$$

respectively, where $m_{\mathscr{R}}$ is the mass of $\mathscr{R}$, $\mathbf{I}_{\mathscr{R}}$ is the moment of inertia of $\mathscr{R}$ taken about its centre of mass expressed in $\underrightarrow{\mathscr{F}}_b$, g is the constant acceleration due to gravity and $\mathbf{1}_3 = [0 \;\; 0 \;\; 1]^\mathsf{T}$ [14]. The kinetic and potential energy of $\mathscr{P}$ is,

$$T_{\mathscr{P}} = \tfrac{1}{2}\boldsymbol{\omega}_p^{pi^\mathsf{T}} \mathbf{J}_{\mathscr{P}} \boldsymbol{\omega}_p^{pi}, \tag{10}$$

and

$$V_{\mathscr{P}} = -\tfrac{1}{2} m_{\mathscr{P}} g \boldsymbol{l}_p^\mathsf{T} \mathbf{C}_{pi} \mathbf{1}_3, \tag{11}$$

respectively, where $m_{\mathscr{P}}$ is the mass of $\mathscr{P}$ and $\mathbf{J}_{\mathscr{P}}$ is the moment of inertia of $\mathscr{P}$ taken about the centre of $\underrightarrow{\mathscr{F}}_p$ with respect to $\underrightarrow{\mathscr{F}}_p$. Combining Eqs. (8) and (10) we obtain the expression for the total kinetic energy as

$$\begin{aligned} T &= \tfrac{1}{2} m_{\mathscr{R}} \dot{\mathbf{r}}_i^{bi^\mathsf{T}} \dot{\mathbf{r}}_i^{bi} + \tfrac{1}{2} \boldsymbol{\omega}_b^{bi^\mathsf{T}} \mathbf{I}_{\mathscr{R}} \boldsymbol{\omega}_b^{bi} + \tfrac{1}{2} \boldsymbol{\omega}_p^{pi^\mathsf{T}} \mathbf{J}_{\mathscr{P}} \boldsymbol{\omega}_p^{pi} \\ &= \tfrac{1}{2} \begin{bmatrix} \dot{\mathbf{r}}_b^{bi^\mathsf{T}} & \boldsymbol{\omega}_b^{bi^\mathsf{T}} & \boldsymbol{\omega}_p^{pi^\mathsf{T}} \end{bmatrix}^\mathsf{T} \underbrace{\begin{bmatrix} m_{\mathscr{P}}\mathbf{1} & \mathbf{0} & \mathbf{0} \\ \mathbf{0} & \mathbf{I}_{\mathscr{R}} & \mathbf{0} \\ \mathbf{0} & \mathbf{0} & \mathbf{J}_{\mathscr{P}} \end{bmatrix}}_{\mathbf{M}} \begin{bmatrix} \dot{\mathbf{r}}_b^{bi} \\ \boldsymbol{\omega}_b^{bi} \\ \boldsymbol{\omega}_p^{pi} \end{bmatrix} \\ &= \tfrac{1}{2} \boldsymbol{\nu}^\mathsf{T} \mathbf{M} \boldsymbol{\nu}. \end{aligned}$$

Similarly, combining Eqs. (9) and (11) gives the total potential energy,

$$V = -m_{\mathscr{R}} g \mathbf{r}_i^{bi^\mathsf{T}} \mathbf{1}_3 - \tfrac{1}{2} m_{\mathscr{P}} g \boldsymbol{l}_p^\mathsf{T} \mathbf{C}_{pi} \mathbf{1}_3 \tag{12}$$

It remains to express T in terms of the generalized coordinates. Recalling Eq. (1), T can be rewritten as

$$T = \tfrac{1}{2} \dot{\mathbf{q}}^\mathsf{T} \mathbf{S}^\mathsf{T} \mathbf{M} \mathbf{S} \dot{\mathbf{q}}, \tag{13}$$

where

$$\mathbf{S} = \begin{bmatrix} \mathbf{1} & \mathbf{0} & \mathbf{0} \\ \mathbf{0} & \mathbf{S}_b^{bi} & \mathbf{0} \\ \mathbf{0} & \mathbf{0} & \mathbf{S}_p^{pi} \end{bmatrix}.$$

Now, the lagrangian can be formed as

$$L = T - V = \tfrac{1}{2} \dot{\mathbf{q}}^\mathsf{T} \mathbf{S}^\mathsf{T} \mathbf{M} \mathbf{S} \dot{\mathbf{q}} + m_{\mathscr{R}} g \mathbf{r}_i^{bi^\mathsf{T}} \mathbf{1}_3 + \tfrac{1}{2} m_{\mathscr{P}} g \boldsymbol{l}_p^\mathsf{T} \mathbf{C}_{pi} \mathbf{1}_3.$$

Generalized Torques

The only external torques that will be considered in our model is $\boldsymbol{\tau}_d \in \mathbb{R}^3$, that is the torque induced on the platform by the wind and the disturbance that the flight train induces on the platform. To find $\boldsymbol{\tau}_d$ the method of virtual work will be employed [13]. The virtual work done due to the disturbance torque is

$$\begin{aligned} \delta W &= \underrightarrow{\tau}_d \cdot \underrightarrow{\mathscr{F}}_b^\mathsf{T} \mathbf{S}_b^{bi} \delta \boldsymbol{\theta}^{bi} \\ &= \delta \mathbf{q}^\mathsf{T} \mathbf{S}^\mathsf{T} \underbrace{\begin{bmatrix} \mathbf{0} \\ \boldsymbol{\tau}_d \\ \mathbf{0} \end{bmatrix}}_{\bar{\boldsymbol{\tau}}_d} \\ &= \delta \mathbf{q}^\mathsf{T} \mathbf{S}^\mathsf{T} \bar{\boldsymbol{\tau}}_d, \end{aligned}$$

where $\mathbf{S}^{\mathsf{T}}\bar{\boldsymbol{\tau}}_d$ is the generalized disturbance torque. We will also consider, $\boldsymbol{\tau}_c \in \mathbb{R}^3$, a control torque produced by actuators onboard the platform. The virtual work done due to the control torque is

$$\begin{aligned}\delta W &= \underrightarrow{\tau}_c \cdot \underrightarrow{\mathscr{F}}_b^{\mathsf{T}} \mathbf{S}_b^{bi} \delta\boldsymbol{\theta}^{bi} \\ &= \delta\mathbf{q}^{\mathsf{T}}\mathbf{S}^{\mathsf{T}} \begin{bmatrix} \mathbf{0} \\ \boldsymbol{\tau}_c \\ \mathbf{0} \end{bmatrix} \\ &= \delta\mathbf{q}^{\mathsf{T}}\mathbf{S}^{\mathsf{T}}\bar{\boldsymbol{\tau}}_c,\end{aligned}$$

where $\mathbf{S}^{\mathsf{T}}\bar{\boldsymbol{\tau}}_c$ is the generalized torque due to the onboard actuators.

Equations of Motion

Omitting details for brevity, Eq. (6) gives

$$\mathbf{S}^{\mathsf{T}}\left(\mathbf{M}\dot{\boldsymbol{\nu}} + \boldsymbol{\Omega}\mathbf{M}\boldsymbol{\nu} + \mathbf{a}\right) = \boldsymbol{\Xi}^{\mathsf{T}}\boldsymbol{\lambda} + \mathbf{S}^{\mathsf{T}}(\bar{\boldsymbol{\tau}}_d + \bar{\boldsymbol{\tau}}_c), \tag{14}$$

where

$$\boldsymbol{\Omega} = \begin{bmatrix} \mathbf{0} & \mathbf{0} & \mathbf{0} \\ \mathbf{0} & \boldsymbol{\omega}_b^{bi\times} & \mathbf{0} \\ \mathbf{0} & \mathbf{0} & \boldsymbol{\omega}_p^{pi\times} \end{bmatrix}, \quad \text{and} \quad \mathbf{a} = \begin{bmatrix} -m_{\mathscr{R}} g \mathbf{1}_3 \\ \mathbf{0} \\ -\frac{1}{2} m_{\mathscr{P}} g \boldsymbol{l}_b^{\times} \mathbf{C}_{pi} \mathbf{1}_3 \end{bmatrix}.$$

3.3. Expressing the Equations of Motion in Terms of the Independent Generalized Coordinates

We have derived the equations of motion in terms of the dependent generalized coordinates, $\boldsymbol{\nu}$. We will now employ the *null space method* [13], also known as the natural orthogonal compliment [15, 16], to express the equations of motion in terms of the independent generalized coordinates, $\tilde{\boldsymbol{\nu}}$. This will allow us to avoid calculating the Lagrange multipliers, $\boldsymbol{\lambda}$, as well as reducing the number of states that must be integrated during simulation [13].

Multiplying Eq. (14) by $\boldsymbol{\Gamma}^{\mathsf{T}}$ and recalling from Eq. (5) that $\boldsymbol{\Gamma}^{\mathsf{T}}\boldsymbol{\Xi}^{\mathsf{T}} = \mathbf{0}$ yields

$$\boldsymbol{\Gamma}^{\mathsf{T}}\mathbf{S}^{\mathsf{T}}\left(\mathbf{M}\dot{\boldsymbol{\nu}} + \boldsymbol{\Omega}\mathbf{M}\boldsymbol{\nu} + \mathbf{a}\right) = \boldsymbol{\Gamma}^{\mathsf{T}}\mathbf{S}^{\mathsf{T}}(\bar{\boldsymbol{\tau}}_d + \bar{\boldsymbol{\tau}}_c). \tag{15}$$

Simplifying $\boldsymbol{\Gamma}^{\mathsf{T}}\mathbf{S}^{\mathsf{T}}$, we find that

$$\begin{aligned}\boldsymbol{\Gamma}^{\mathsf{T}}\mathbf{S}^{\mathsf{T}} &= \begin{bmatrix} (\mathbf{C}_{bi}^{\mathsf{T}}\mathbf{y}_b^{\times}\mathbf{S}_b^{bi})^{\mathsf{T}} & \mathbf{1} & \mathbf{0} \\ (-\mathbf{C}_{pi}^{\mathsf{T}}\boldsymbol{l}_p^{\times}\mathbf{S}_p^{pi})^{\mathsf{T}} & \mathbf{0} & \mathbf{1} \end{bmatrix} \begin{bmatrix} \mathbf{1} & \mathbf{0} & \mathbf{0} \\ \mathbf{0} & \mathbf{S}_b^{bi^{\mathsf{T}}} & \mathbf{0} \\ \mathbf{0} & \mathbf{0} & \mathbf{S}_p^{pi^{\mathsf{T}}} \end{bmatrix} \\ &= \begin{bmatrix} (\mathbf{C}_{bi}^{\mathsf{T}}\mathbf{y}_b^{\times}\mathbf{S}_b^{bi})^{\mathsf{T}} & \mathbf{S}_b^{bi^{\mathsf{T}}} & \mathbf{0} \\ (-\mathbf{C}_{pi}^{\mathsf{T}}\boldsymbol{l}_p^{\times}\mathbf{S}_p^{pi})^{\mathsf{T}} & \mathbf{0} & \mathbf{S}_p^{pi^{\mathsf{T}}} \end{bmatrix} \\ &= \underbrace{\begin{bmatrix} \mathbf{S}_b^{bi^{\mathsf{T}}} & \mathbf{0} \\ \mathbf{0} & \mathbf{S}_p^{pi^{\mathsf{T}}} \end{bmatrix}}_{\tilde{\mathbf{S}}^{\mathsf{T}}} \underbrace{\begin{bmatrix} -\mathbf{y}_b^{\times}\mathbf{C}_{bi} & \mathbf{1} & \mathbf{0} \\ \boldsymbol{l}_p^{\times}\mathbf{C}_{pi} & \mathbf{0} & \mathbf{1} \end{bmatrix}}_{\boldsymbol{\Delta}} \qquad (16) \\ &= \tilde{\mathbf{S}}^{\mathsf{T}}\boldsymbol{\Delta}. \qquad (17)\end{aligned}$$

Substituting Eq. (4) and Eq. (17) into Eq. (15), and premultiplying by $\tilde{\mathbf{S}}^{-\mathsf{T}}$ gives

$$\boldsymbol{\Delta}(\mathbf{M}\boldsymbol{\Pi}\dot{\tilde{\boldsymbol{\nu}}} + \mathbf{M}\dot{\boldsymbol{\Pi}}\tilde{\boldsymbol{\nu}} + \boldsymbol{\Omega}\mathbf{M}\boldsymbol{\Pi}\tilde{\boldsymbol{\nu}} + \mathbf{a}) = \boldsymbol{\Delta}(\bar{\boldsymbol{\tau}}_d + \bar{\boldsymbol{\tau}}_c), \tag{18}$$

where

$$\dot{\boldsymbol{\Pi}} = \begin{bmatrix} \mathbf{C}_{bi}^{\mathsf{T}}\boldsymbol{\omega}_b^{bi\times}\mathbf{y}_b^{\times} & -\mathbf{C}_{pi}^{\mathsf{T}}\boldsymbol{\omega}_p^{pi\times}\boldsymbol{l}_p^{\times} \\ \mathbf{0} & \mathbf{0} \\ \mathbf{0} & \mathbf{0} \end{bmatrix}.$$

We let $\tilde{\mathbf{M}}(\boldsymbol{\theta}^{bi}, \boldsymbol{\theta}^{pi}) = \boldsymbol{\Delta}\mathbf{M}\boldsymbol{\Pi}$, $\tilde{\boldsymbol{\tau}}_{non} = \boldsymbol{\Delta}\left(\mathbf{M}\dot{\boldsymbol{\Pi}}\tilde{\boldsymbol{\nu}} + \boldsymbol{\Omega}\mathbf{M}\boldsymbol{\Pi}\tilde{\boldsymbol{\nu}} + \mathbf{a}\right)$, $\tilde{\boldsymbol{\tau}}_w = \boldsymbol{\Delta}\bar{\boldsymbol{\tau}}_d$ and $\tilde{\boldsymbol{\tau}}_c = \boldsymbol{\Delta}\bar{\boldsymbol{\tau}}_c$, then the equations of motion in terms of the independent generalized coordinates can be written as

$$\tilde{\mathbf{M}}(\boldsymbol{\theta}^{bi}, \boldsymbol{\theta}^{pi})\dot{\tilde{\boldsymbol{\nu}}} + \tilde{\boldsymbol{\tau}}_{non} = \tilde{\boldsymbol{\tau}}_w + \tilde{\boldsymbol{\tau}}_c. \tag{19}$$

To validate these equations a simulation was conducted with zero disturbances and non-zero initial conditions to verify that the energy of the system remained constant.

4. ESTIMATION

Recall from Eq. (2), the kinematics of $\mathscr{R}$ obey [2]

$$\dot{\mathbf{C}}_{bi} = -\boldsymbol{\omega}_b^{bi\times}\mathbf{C}_{bi}.$$

For the sake of simplicity in notation, we will now neglect to write the subscripts and superscripts such that the above can be rewritten as

$$\dot{\mathbf{C}} = -\boldsymbol{\omega}^{\times}\mathbf{C}.$$

Let $\underrightarrow{g}$ and $\underrightarrow{m}$ be the direction unit vectors corresponding to the Earth's gravitational acceleration and magnetic field respectively. We measure $\underrightarrow{g}$ and $\underrightarrow{m}$ in the body frame. Therefore we have,

$$\mathbf{g}_b^y = \mathbf{C}\mathbf{g}_i + \boldsymbol{\mu}_g \quad \text{and} \quad \mathbf{m}_b^y = \mathbf{C}\mathbf{m}_i + \boldsymbol{\mu}_m,$$

where $\mathbf{g}_b^y \in \mathbb{R}^3$ and $\mathbf{m}_b^y \in \mathbb{R}^3$ are normalized and correspond to the measurements expressed in the body frame, and $\boldsymbol{\mu}_g \in \mathbb{R}^3$ and $\boldsymbol{\mu}_m \in \mathbb{R}^3$ are zero mean Gaussian noise associated with the measurements. We assume $\boldsymbol{\mu}_g \sim \mathscr{N}(\mathbf{0}, \mathbf{R}_g)$ and $\boldsymbol{\mu}_m \sim \mathscr{N}(\mathbf{0}, \mathbf{R}_m)$. We also measure angular velocity,

$$\boldsymbol{\omega}^y = \boldsymbol{\omega} + \boldsymbol{\mu}_\omega,$$

where $\boldsymbol{\omega}^y = [\omega_1^y \;\; \omega_2^y \;\; \omega_3^y]^{\mathsf{T}}$ is the measured angular velocity and $\boldsymbol{\mu}_\omega \sim \mathscr{N}(\mathbf{0}, \mathbf{R}_\omega)$ is the noise associated with the gyroscope measurement. We will now implement the estimator dynamics proposed in [7]. Let

$$\dot{\hat{\mathbf{C}}} = -(\boldsymbol{\omega}^y + \boldsymbol{\sigma})^{\times}\hat{\mathbf{C}} = -\hat{\boldsymbol{\omega}}^{\times}\hat{\mathbf{C}}$$

where $\hat{\boldsymbol{\omega}} = \boldsymbol{\omega}^y + \boldsymbol{\sigma}$, $\hat{\mathbf{C}}$ is the estimate of $\mathbf{C}$, and $\boldsymbol{\sigma}$ is the innovation. The goal is to drive $\hat{\mathbf{C}}$ to $\mathbf{C}$. We will choose $\boldsymbol{\sigma}$ as [7, 9],

$$\boldsymbol{\sigma} = -k\left(k_g\hat{\mathbf{g}}_b^{\times}\mathbf{g}_b^y + k_m\hat{\mathbf{m}}_b^{\times}\mathbf{m}_b^y\right),$$

where

$$\hat{\mathbf{g}}_b = \hat{\mathbf{C}}\mathbf{g}_i \quad \text{and} \quad \hat{\mathbf{m}}_b = \hat{\mathbf{C}}\mathbf{m}_i,$$

are the estimates of $\mathbf{g}_i$ and $\mathbf{m}_i$ expressed in the body frame, and $0 < k < \infty$, $0 < k_g < \infty$ and $0 < k_m < \infty$ are constants.

In practise, the estimation will be done in discrete time, therefore it is necessary to discretize the estimator dynamics. Let T denote the sample time and assume that $\hat{\boldsymbol{\omega}} = \hat{\boldsymbol{\omega}}^k$ for $t \in [kT, (k+1)T]$ then the discrete time estimator dynamics are given by [7, 9],

$$\hat{\mathbf{C}}^{k+1} = \mathbf{A}^k \hat{\mathbf{C}}^k,$$

where $\mathbf{A}^k = \exp(\hat{\boldsymbol{\omega}}^{k^\times})$ is given by [11]

$$\mathbf{A}^k = \mathbf{1} - \hat{\boldsymbol{\omega}}^{k^\times} \frac{\sin(|\hat{\boldsymbol{\omega}}^k|T)}{|\hat{\boldsymbol{\omega}}^k|} + \left(\hat{\boldsymbol{\omega}}^{k^\times}\right)^2 \frac{1-\cos(|\hat{\boldsymbol{\omega}}^k|T)}{|\hat{\boldsymbol{\omega}}^k|^2}.$$

5. CONTROL

The atmospheric balloon platform is equipped with only one actuator to control the yaw angle of the platform. Therefore, let $\boldsymbol{\tau}_c = [0 \;\; 0 \;\; \tau_c]^\mathsf{T}$. Now, consider the following PD type control law:

$$\tau_c = -k_p \hat{\theta}_3 - k_d \omega_3^y,$$

where $\hat{\theta}_3$ is the estimated yaw angle of the platform extracted from $\hat{\mathbf{C}}$, ω_3^y is the third component of the measured angular velocity, and k_p and k_d are constants such that $0 < k_p < \infty$ and $0 < k_d < \infty$.

6. DISTURBANCE MODEL

We will model the platform dynamics using a Runge-Kutta integrator with a fine time step. Since we have included the disturbances in the truth model, it is necessary to find a continuous-time model for the disturbances. To do this, we will consider the disturbances to be a zero mean Gaussian process. A stochastic process, $f(x)$, is said to be zero mean and Gaussian if for any choice of $\mathbf{x} = [x_1 \;\; x_2 \;\; \dots \;\; x_n]^\mathsf{T}$ the vector $\mathbf{f} = [f(x_1) \;\; f(x_2) \;\; \dots \;\; f(x_n)]^\mathsf{T}$ has a zero mean Gaussian distribution [17]. That is, $\mathbf{f} \sim \mathcal{N}(\mathbf{0}, \mathbf{K})$, where $\mathbf{K} = \mathrm{E}[\mathbf{f}\mathbf{f}^\mathsf{T}]$ is the covariance matrix. We will denote a Gaussian process as

$$f(x) \sim \mathcal{GP}\left(m(x), k(x,x')\right),$$

where $f(x)$ is completely described by its mean function, $m(x) = \mathrm{E}[f(x)]$, and its covariance function, $k(x,x') = \mathrm{E}[f(x)f(x')]$ [17]. Note, the relationship between $k(x,x')$ and $\mathbf{K}$ is

$$\mathbf{K} = \begin{bmatrix} k(x_1,x_1) & k(x_1,x_2) & \cdots & k(x_1,x_n) \\ k(x_2,x_1) & k(x_2,x_2) & \cdots & k(x_2,x_n) \\ \vdots & \vdots & \ddots & \vdots \\ k(x_n,x_1) & k(x_n,x_2) & \cdots & k(x_n,x_n) \end{bmatrix}. \tag{20}$$

We wish to find $\tau_d(t) \sim \mathcal{GP}(0, k(t,t'))$ such that we can choose $\mathbf{t} = [t_1 \;\; t_2 \;\; \dots \;\; t_n]^\mathsf{T}$ s, where t_n is the length of the simulation, and construct a vector of disturbances, $\boldsymbol{\tau} \in \mathbb{R}^{n\times 1} \sim \mathcal{N}(\mathbf{0}, \mathbf{K})$. To this end, we select

$$k(t,t') = \sigma^2 \exp\left(-\frac{|t-t'|^2}{2l^2}\right),$$

where σ^2 is the desired variance of the disturbance and l is a characteristic length-scale [17]. Now, we can construct the covariance matrix, $\mathbf{K}$, from Eq. (20). To generate the disturbance sample we decompose $\mathbf{K}$ into its eigenvalue decomposition, $\mathbf{K} = \mathbf{E}\boldsymbol{\Lambda}\mathbf{E}^{-1}$, and set

$$\boldsymbol{\tau} = \mathbf{E}\mathbf{v},$$

where $\mathbf{v} = \boldsymbol{\Lambda}^{\frac{1}{2}}\mathbf{w}$ and $\mathbf{w}$ is a vector of random variables such that $\mathbf{w} \sim \mathcal{N}(\mathbf{0}, \mathbf{1})$ [18]. We have generated a vector of disturbances, $\boldsymbol{\tau} = [\tau_d(t_1) \;\; \tau_d(t_2) \;\; \ldots \;\; \tau_d(t_n)]^\mathsf{T}$, corresponding to each time in $\mathbf{t}$. However, during simulation, we may need to evaluate $\tau_d(t)$ at any arbitrary time, t_*. In this case,

$$\tau_d(t_*) = \mathbf{K}_*\mathbf{K}^{-1}\boldsymbol{\tau},$$

where $\mathbf{K}_* = [k(t_*,t_1) \;\; k(t_*,t_2) \;\; \ldots \;\; k(t_*,t_n)]$ [17]. Note that this disturbance model is based heuristically on actual flight data. This is a low fidelity model as there remain many unmodelled effects. However, it is sufficient for an initial investigation.

7. SIMULATION RESULTS

The estimation algorithm and control law presented above will now be implemented in a simulation of the balloon platform. The physical properties of the platform and pendulum system are shown in Table 1. The initial angular velocity is $\boldsymbol{\omega}_0 = [0 \;\; 0 \;\; 0.1]^\mathsf{T}$ rad/s and the initial attitude is $\mathbf{C}_{bi,0} = \mathbf{C}_1(0^\circ)\mathbf{C}_2(0^\circ)\mathbf{C}_3(20^\circ)$, where $\mathbf{C}_i$, $i = 1,\ 2,\ 3$ are principal rotations about the 1, 2 and 3 axes. The desired attitude of the platform is $\mathbf{C}_d = \mathbf{C}_1(\theta_1)\mathbf{C}_2(\theta_2)\mathbf{C}_3(0^\circ)$ where θ_1 and θ_2 are arbitrary. The initial pendulum attitude is $\mathbf{C}_{pi,0} = \mathbf{C}_1(-88^\circ)\mathbf{C}_2(0^\circ)\mathbf{C}_3(0^\circ)$ and its initial angular velocity is $\boldsymbol{\omega}_{p,0} = [0 \;\; 0 \;\; 0]^\mathsf{T}$. For the disturbance model, we set $\sigma = 0.05\ N \cdot m$ and $l = 0.3\ s$. During simulation, this plant model is numerically integrated using a fourth-order Runge-Kutta integrator with a time-step of 0.005 s.

Property	Value	Units
$\boldsymbol{l}_p$	$[0 \;\; 2 \;\; 0]^\mathsf{T}$	m
$\mathbf{y}_b$	$[0 \;\; 0 \;\; 0.0577]^\mathsf{T}$	m
$m_{\mathscr{R}}$	6	kg
$\mathbf{I}_{\mathscr{R}}$	$\mathrm{diag}\{0.0161, 0.0163, 0.0112\}$	$kg \cdot m^2$
$m_{\mathscr{P}}$	0.1	kg
$J_{\mathscr{P}}$	$\mathrm{diag}\{0.133,\ 5 \cdot 10^{-6},\ 0.133\}$	$kg \cdot m^2$

Table 1. Physical properties of the platform model

For the observer, we set $k = 1$, $k_g = 1$ and $k_m = 0.5$. The initial estimate of the attitude is $\hat{\mathbf{C}}_0 = \mathbf{1}$. The measurement noise covariance matrices associated with the accelerometer, magnetometer and gyroscope are $\mathbf{R}_g = \mathrm{diag}\{\sigma_g^2,\ \sigma_g^2,\ \sigma_g^2\}$, $\mathbf{R}_m = \mathrm{diag}\{\sigma_m^2,\ \sigma_m^2,\ \sigma_m^2\}$ and $\mathbf{R}_\omega = \mathrm{diag}\{\sigma_\omega^2,\ \sigma_\omega^2,\ \sigma_\omega^2\}$ respectively, where $\sigma_g = \sigma_\omega = 0.005$ and $\sigma_m = 0.01$. We will assume that $\mathbf{g}_i = [0 \;\; 0 \;\; -1]^\mathsf{T}$ and $\mathbf{m}_i = 1/\sqrt{3}[1 \;\; 1 \;\; 1]^\mathsf{T}$ for all time. The control gains are set to $k_p = 6$ and $k_d = 0.25$. We will consider the estimation and control algorithms to be running on an onboard computer at a frequency of 25 Hz. Therefore, during the simulation the measurements are acquired and the control commands are updated every 0.04 s.

The Euler angles as well as their estimates are shown in Fig. 2(a). Note that the estimates converge to their true counterparts and that the yaw angle of the platform approaches 0°, its desired value. The angular velocity of the balloon platform is shown in Fig. 2(b). Since no viscous drag has been modelled there is no

damping in the pitch and roll angles and they continue to swing. Although the yaw angle of the platform approaches zero, its angular velocity is unsteady due to the high disturbance torques. The control torque, τ_c, and the disturbance torque, τ_d, are shown in Fig. 3. The control torque mirrors the disturbances almost exactly. In the future, a more aggressive control law with higher control authority over the disturbances should be implemented.

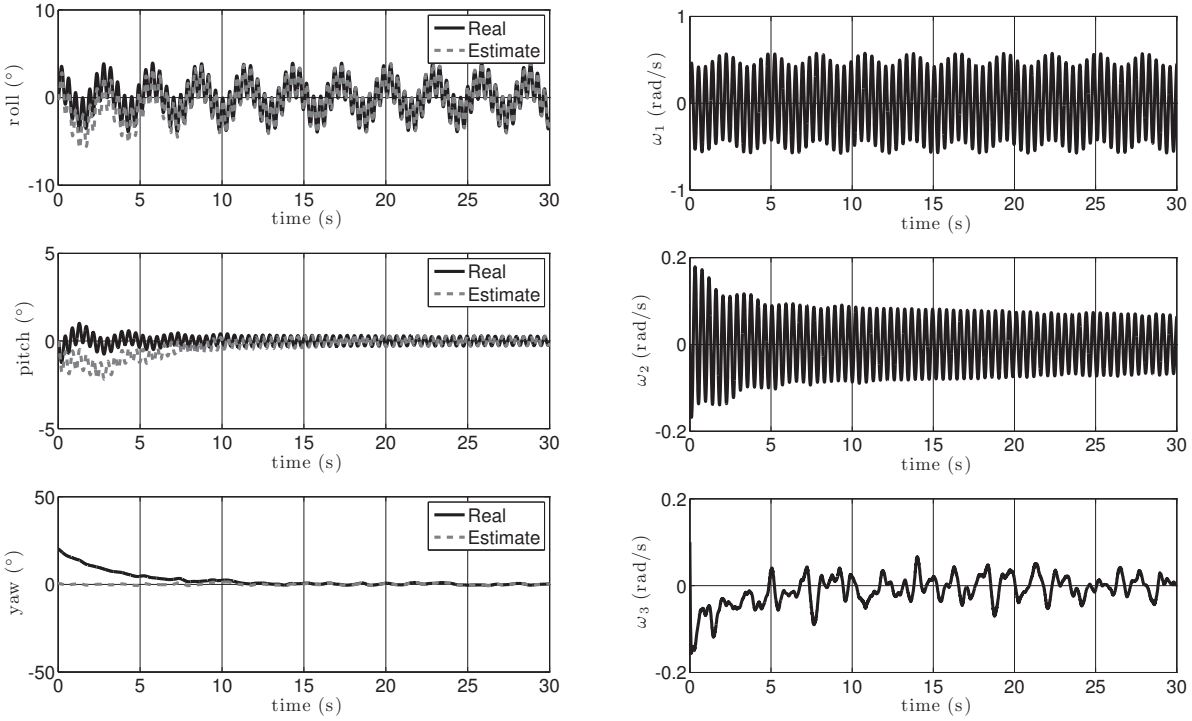

(a) (b)

Fig. 2. (a) Euler angles and (b) angular velocity versus time

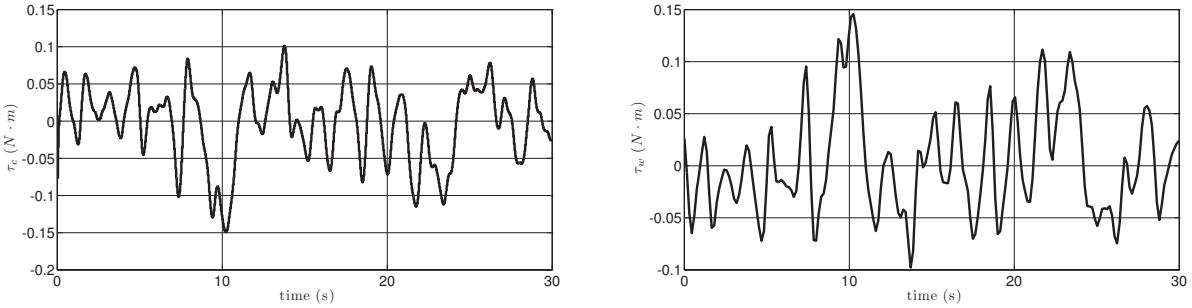

(a) (b)

Fig. 3. (a) Control and (b) disturbance torques versus time

8. CONCLUSIONS

In this paper the dynamic modelling, estimation, and control of an atmospheric balloon platform has been investigated. We have derived the equations of motion of the balloon platform and included the effects of a

continuous-time disturbance torque. Accelerometer, magnetometer and gyroscope measurements were used to construct the estimator proposed in [7, 9], and a simple PD control law was implemented to control the yaw angle of the platform. As mentioned in Sec. 1, the contribution of this work is the implementation of the estimator in combination with yaw control on an atmospheric balloon platform system. It was shown, through numerical simulation, that the estimator converged to the true state values and the yaw angle of the platform was successfully controlled.

REFERENCES

1. Wertz, J.R. *Spacecraft Attitude Determination and Control*. D. Reidel Publishing Company, Dordrecht, The Netherlands, 1978.
2. Hughes, P.C. *Spacecraft Attitude Dynamics*. Second ed.. Dover, Mineola, New York, 2004.
3. Crassidis, J.L. and Junkins, J.L. *Optimal Estimation of Dynamic Systems*. Second ed.. CRC Press, Taylor and Francis Group, Boca Raton, FL, 2012.
4. Quine, B.M., Strong, K., Wiacek, A., Wunch, D., Anstey, J.A. and Drummond, J.R. "Scanning the Earth's limb from a high-altitude balloon: the development and flight of a new balloon-based pointing system." *Journal of Atmospheric and Oceanic Technology*, Vol. 19, No. 5, pp. 618–632, 2002.
5. Pascale, E., Ade, P., Bock, J., Chapin, E., Chung, J., Devlin, M., Dicker, S., Griffin, M., Gundersen, J., Halpern, M. et al.. "The balloon-borne large aperture submillimeter telescope: BLAST." *The Astrophysical Journal*, Vol. 681, No. 1, p. 400, 2008.
6. Buccilli, T., Folina, A., Medaglia, E., Montefusco, P., Oliva, M., Palmerini, G. and Sestito, A. "A low cost inertial navigation experiment onboard balloons." *Proc. of the 19th ESA Symposium on European Rocket and Balloon Programmes and Related Research, Bad Reichenhall, Germany, 2009*.
7. Mahony, R., Hamel, T. and Pflimlin, J.M. "Complementary filter design on the special orthogonal group SO(3)." *Proc. of the IEEE Conf. on Decision and Control, and the European Control Conf., Seville, Spain, December 12-15, 2005*, pp. 1477–1484. MoC03.3.
8. Khosravian, A. and Namvar, M. "Globally exponential estimation of satellite attitude using a single vector measurement and gyro." *Proc. of the IEEE Conf. on Decision and Control, Atlanta, GA, December 15-17, 2010*, pp. 364–369.
9. Hamel, T. and Mahony, R. "Attitude estimation on SO(3) based on direct inertial measurements." *Proc. of the IEEE International Conf. on Robotics and Automation, Orlando, FL, May 15-19, 2006*, pp. 2170–2175.
10. Mahony, R., Hamel, T. and Pflimlin, J.M. "Nonlinear complementary filters on the special orthogonal group." *IEEE Transactions on Automatic Control*, Vol. 53, No. 5, pp. 1203–1218, June 2008.
11. Murray, R., Li, Z. and Sastry, S. *A mathematical Introduction to Robotic Manipulation*. CRC, 1994.
12. Tran, N.K., He, X., Zlotnik, D.E. and Forbes, J.R. *Attitude Sensing and Control of a Stratospheric Ballon Platform*. American Institute of Aeronautics and Astronautics, 2013.
13. Forbes, J., Barfoot, T. and Damaren, C. "Dynamic modeling and stability analysis of a power-generating tumbleweed rover." *Multibody System Dynamics*, Vol. 24, pp. 413–439, 2010.
14. Chaturvedi, N., Lee, T., Leok, M. and McClamroch, N. "Nonlinear dynamics of the 3D pendulum." *Journal of Nonlinear Science*, Vol. 21, No. 1, pp. 3–32, 2011.
15. De Jalon, J.G. and Bayo, E. *Kinematic and dynamic simulation of multibody systems*. Springer-Verlag, 1994.
16. Angeles, J. and LEE, S. "The modelling of holonomic mechanical systems using a natural orthogonal complement." *Canadian Society for Mechanical Engineering, Transactions*, Vol. 13, No. 4, pp. 81–89, 1989.
17. Rasmussen, C.E. and Williams, C.K. *Gaussian processes for machine learning*, Vol. 1. MIT press Cambridge, MA, 2006.
18. de Ruiter, A., Damaren, C. and Forbes, J. *Spacecraft Dynamics and Control: An Introduction*. Wiley, Chichester West Sussex, UK, 2013.